Steel and Composite Structures, *Vol. 30, No. 6 (2019) 535-550*
DOI: https://doi.org/10.12989/scs.2019.30.6.535

Comparison of long-term behavior between prestressed concrete and corrugated steel web bridges

Yulin Zhan [*1], Fang Liu [1a], Zhongguo John Ma [2b], Zhiqiang Zhang [1c], Zengqiang Duan [1d] and Ruinian Song [1e]

[1] *Department of Bridge Engineering, School of Civil Engineering, Southwest Jiaotong University, Sichuan 610031, China*
[2] *Department of Civil and Environmental Engineering, University of Tennessee, Knoxville, John D.Tickle, TN 37996-2313, USA*

(*Received January 20, 2018, Revised January 4, 2019, Accepted March 9, 2019*)

Abstract. Prestressed concrete (PC) bridges using corrugated steel webbing have emerged as one of the most promising forms of steel-concrete composite bridge. However, their long-term behavior is not well understood, especially in the case of large-span bridges. In order to study the time-dependent performance, a large three-span PC bridge with corrugated steel webbing was compared to a similar conventional PC bridge to examine their respective time-dependent characteristics. In addition, a three-dimensional finite element method with step-by-step time integration that takes into account cantilever construction procedures was used to predict long-term behaviors such as deflection, stress distribution and prestressing loss. These predictions were based upon four well-established empirical creep prediction models. PC bridges with a corrugated steel web were observed to have a better long-term performance relative to conventional PC bridges. In particular, it is noted that the pre-cambering for PC bridges with a corrugated steel web could be smaller than that of conventional PC bridges. The ratio of side-to-mid span has great influence on the long-term deformation of PC bridges with a corrugated steel web, and it is suggested that the design value should be between 0.4 and 0.6. However, the different creep prediction models still showed a weak homogeneity, thus, the further experimental research and the development of health monitoring systems are required to further progress our understanding of the long-term behavior of PC bridges with corrugated steel webbing.

Keywords: long-term behavior; prestressed concrete; corrugated steel web; bridge; numerical simulation; creep prediction

1. Introduction

Though conventional prestressed concrete (PC) bridges have been used widely throughout the world, the material possesses weaknesses that limit the scope for using it in the construction of long-span bridges. One such issue is that the dead load of a longer span would increase its moment, placing a limit upon the potential length of a span (Rosignoli 1999, Zhan *et al*. 2016a). A second problem is that prestressing efficiency of PC is reduced when it is used in very large bridge sections (Jiang *et al*. 2015). A third issue is that diagonal cracks are already often observed in existing PC bridge webs that result from insufficient prestressing, excess permanent loads and secondary stresses such as increases in traffic flow and thermal effects (Sprinkel and Balakumaran 2017). This would only be aggravated by an increase in span. In view of this, the PC bridges with corrugated steel webbing have become popular because they offer reduced weight, more efficient prestressing of the concrete flanges and less cracking in the web. This type of bridge has been successfully used in France (Combault 1988), Germany (Roesler and Denzer 2002), Norway (Combault 1988), Korea (Jung *et al*. 2011), Japan (Ikeda *et al*. 2002) and China (Wan *et al*. 2009, Jiang *et al*. 2015). However, most research to date has focused on the short-term behavior of these bridges, such as their flexural performance with regard to the "accordion effect" (Chan *et al*. 2002, Elamary *et al*. 2017, Johnson and Cafolla 1997), shear buckling (Kano *et al*. 1997, Rosignoli 1999) and their torsional behavior (Mo and Fan 2006, Ikeda *et al*. 2002). Little work has been devoted to their longer-term performance, especially when it comes to long-span bridges (Jiang *et al*. 2015, Chen *et al*. 2017). The time-dependent properties of the material, such as relaxation, the adequacy of prestressing, the girder type, and so on, may have an effect upon the long-term behavior of a bridge and result in additional deflection, prestress loss, force redistribution, and possibly cracking.

The long-term behavior of conventional PC bridges has been studied comprehensively (e.g., Bazant *et al*. 2011, 2012a, b, Lou *et al*. 2015, Xiao *et al*. 2014, Geng *et al*. 2014) and most of the results indicate that long-span PC bridges suffer excessive long-term deflection within 20-40 years of their completion (Bazant *et al*. 2011). The long-term behavior of a PC bridge with corrugated steel webbing, however, is more complex because of the existence of the corrugated steel web. Sung *et al*. (2016)

*Corresponding author, Ph.D., Associate Professor, E-mail: yulinzhan@home.swjtu.edu.cn
[a] Graduate Student, E-mail: 1471723936@qq.com
[b] Professor, E-mail: zma2@utk.edu
[c] Graduate Student, E-mail: 2572482089@qq.com
[d] Graduate Student, E-mail: 1356475195@qq.com
[e] Graduate Student, E-mail: ruinian.song@qq.com

ISSN: 1229-9367 (Print), 1598-6233 (Online)

have reported the test results for long-term horizontal shortening, using FEM based on a long-term health monitoring system, for a 93 + 2 × 145 + 93 m PC bridge with corrugated steel webbing in Taiwan. However, the plane section assumption and a Euler-Bernoulli beam were built into this study, undermining the validity of its results. Chen *et al*. (2017) have tested the time-dependent behavior of a simple supporting beam bridge model in a lab. In this case, the PC bridge with corrugated steel webbing was designed to have a span of 2800 mm. In order to make comparisons using FEM, a sandwich element was added to the numerical model. The results showed that the long-term behavior of the bridge was significantly different from traditional PC bridges because of the different type of web. Although a few researchers have begun to study the long-term behavior of PC bridges with corrugated steel webbing, the work is still extremely limited and work relating to long-span PC bridges with corrugated steel webbing is very rare.

In order to tackle this gap in the research, the study reported here has examined the long-term behavior of a three-span innovative PC bridge with corrugated steel webbing that has been constructed in China, with spans of 105 m + 190 m + 105 m. Both PC bridges with corrugated steel webbing and conventional PC bridges were compared in this research across a variety of creep models. On the basis of numerical analysis of the long-term behavior of this type of bridge, this paper presents some design recommendations and suggestions for their health monitoring requirements in the future.

2. A PC bridge with corrugated steel webbing

2.1 Structure

The bridge focused upon in this study was designed as a three-span prestressed concrete bridge with corrugated steel webbing for a highway. An elevation view of the bridge showing the spans and location of various instruments is given in Fig. 1. The bridge is composed of two parts: that is, a beam with corrugated steel webbing through the middle of the spans; and a concrete beam bridge near the supporting piers. The overall span is 105 m + 190 m + 105 m, with the height of the key sections being 11.2m and 5m at the supporting and mid-span points, respectively. The height of the inner piers is 27 m and 31 m. The corrugated web units used in the bridge are 1600 mm in length and 12~25 mm in thickness. Their height and angle are 220 mm and 31°, respectively. C55 and C30 concrete were used, respectively, for the main girder and the piers.

2.2 Prestressing tendons

The layout of the prestressing tendons is shown in Fig. 2. The prestressing tendons consisted of 216 strands of internal tendon and 20 strands of external tendon. The internal prestressing tendons were arranged at the top and bottom flanges of the concrete girders. The external prestressing tendons were assigned to the inner box of the girder, which transfers the prestressing pressure from the

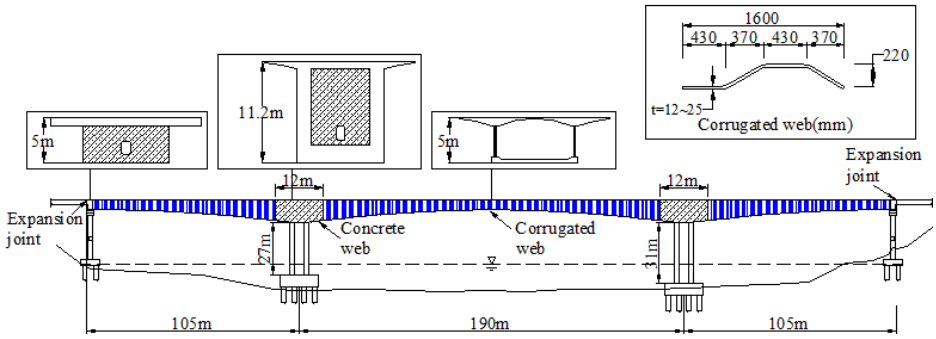

(a) Elevation view

(b) Sketch view

Fig. 1 Layout of the bridge

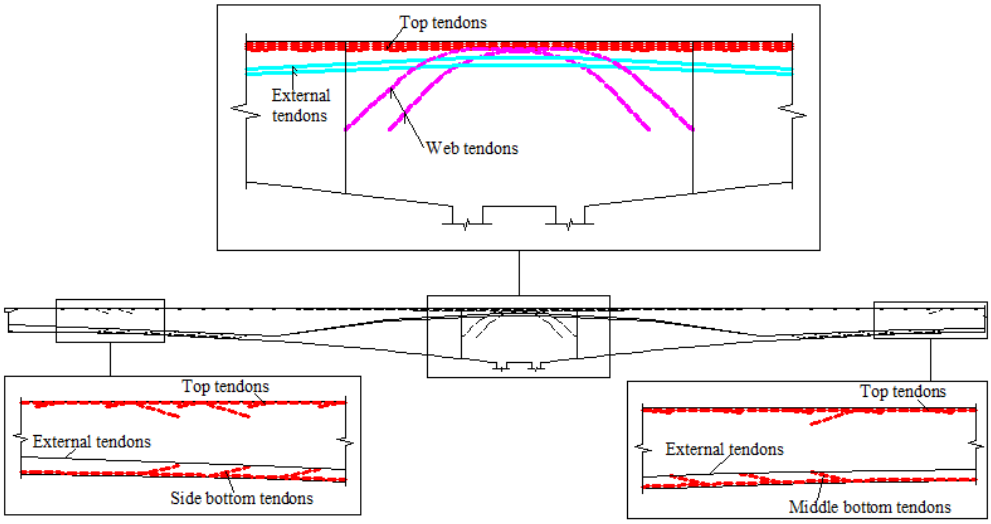

Fig. 2 Arrangement of prestressing tendons of PC bridge with corrugated steel web

tendons to the concrete through end anchors at each end and deviators in the middle span. The internal tendons in the top flange consisted of 21 strands and 23 strands of 15.2 mm in nominal diameter, while the prestressing tendons with 19 strands were used as the internal tendons in the bottom flange. The external tendons consisted of 25 strands of 15.2 mm in nominal diameter. Unlike traditional PC bridges, there are no prestressing tendons in the webbing between the beam segments containing the corrugated steel web, except for the segments above the inner piers.

2.3 Construction stage

The construction stage is summarized in Fig. 3. A cantilever cast-in-place construction of the bridge was carried out where each cantilever was divided into 22 segments, of which the first two segments were made of concrete webs and the rest of corrugated steel webs. The segment lengths were 3.0 m for segment 1 and 2, and the segment lengths were 3.2 m and 4.8 m for segments 3-11 and 12-22, respectively. Four form travelers were used to construct the cantilevered segments symmetrically about the middle piers until the full bridge was finally completed, beginning with the side-spans, then the mid-span. The casting cycle for each single segment was 7 days.

3. Conventional PC bridges

3.1 Structure

To ensure a meaningful comparison with the PC bridge with corrugated steel webbing, a conventional PC bridge was also taken, where the spans were also 105 m + 190 m

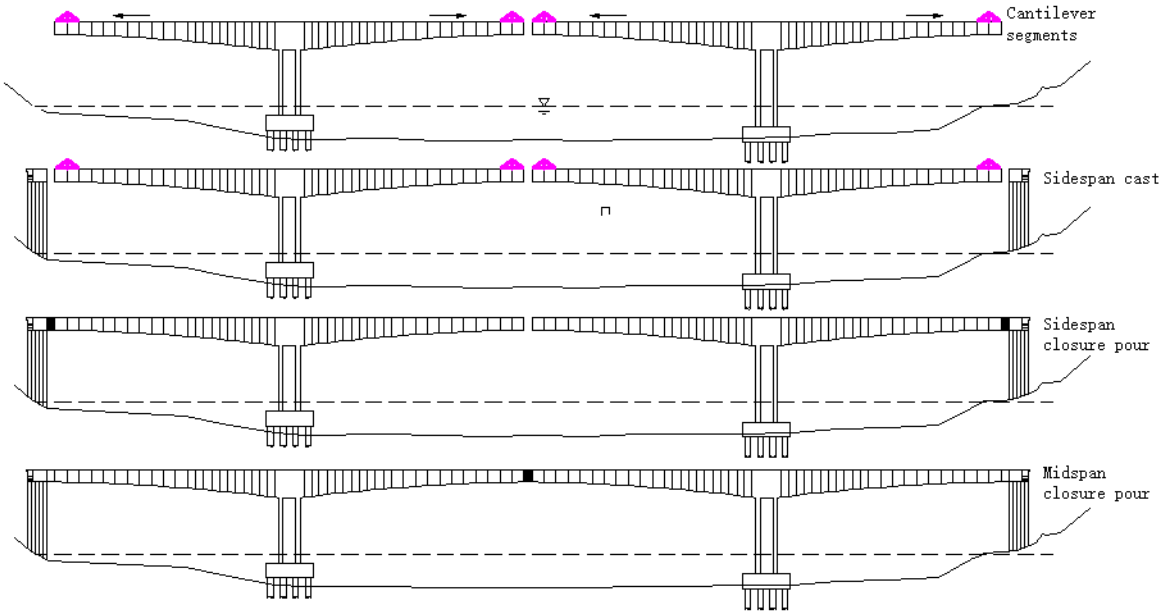

Fig. 3 Construction stages of PC bridge with corrugated steel web

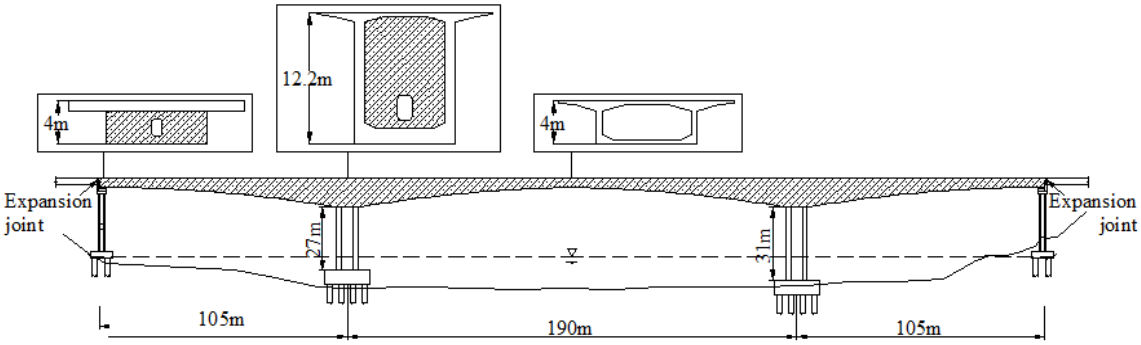

Fig. 4 Elevation view of conventional PC bridge

+ 105 m (see Fig. 4). The principle of comparison adopted was that the moment of resistance for the critical section should be equivalent for both bridges, with the height of the girders and number of prestressing tendons being adjusted accordingly. To simplify the design requirements, the key variables were taken to be the thickness of the webs and the quantity of prestressing tendons (Zhan *et al*. 2016a). After a number of trial calculations, the height near the middle pier and the mid-span was 12.2 m and 4 m, respectively. The thickness of the concrete web varied between 400 mm and 550 mm from the mid-span to the supports at the same locations as in the PC bridge with corrugated steel webbing.

Based on the principle of having an equivalent moment of bending, the quantity of prestressing tendons in the PC bridge was adjusted to between 1.20 and 1.30 times those in the PC bridge with corrugated steel webbing at the critical positions in the top and bottom flanges, respectively. These critical locations included the mid-span, the quarter-span and positions of support. The average moment of resistance at the critical positions under the same loading condition was within a 1% deviation of those in the PC bridge with corrugated steel webbing. A greater amount of prestress was needed because of the structure's relatively high axial stiffness and the potentially greater weight of the webs, as indicated by Chen *et al*. (2017). The arrangement of the prestressing tendons in the PC bridge is shown in Fig. 5.

4. Creep prediction models

4.1 Finite element model

In previous research, the contribution of corrugated webbing to the flexural rigidity of PC bridges was usually set aside because of the so-called "accordion effect" resulting from the bending of thin folded plates (Elgaaly *et al*. 1997, Combault 1998). The assumption that plane sections remain plane had been verified, thereby suggesting that the flexural behavior of both PC bridges with corrugated steel webbing and conventional PC bridges would be similar (Mizuguchi *et al*. 1998, Yamaguchi *et al*. 1997). This meant that either classical Euler-Bernoulli or Timoshenko beam theory could be used to simulate the bridge's bending behavior. However, other researchers have found that the shear deformation of corrugated web cannot be ignored and that the plane section assumption cannot be applied. Machimdamrong *et al*. (2003), for example, discovered that the shear deformation of corrugated

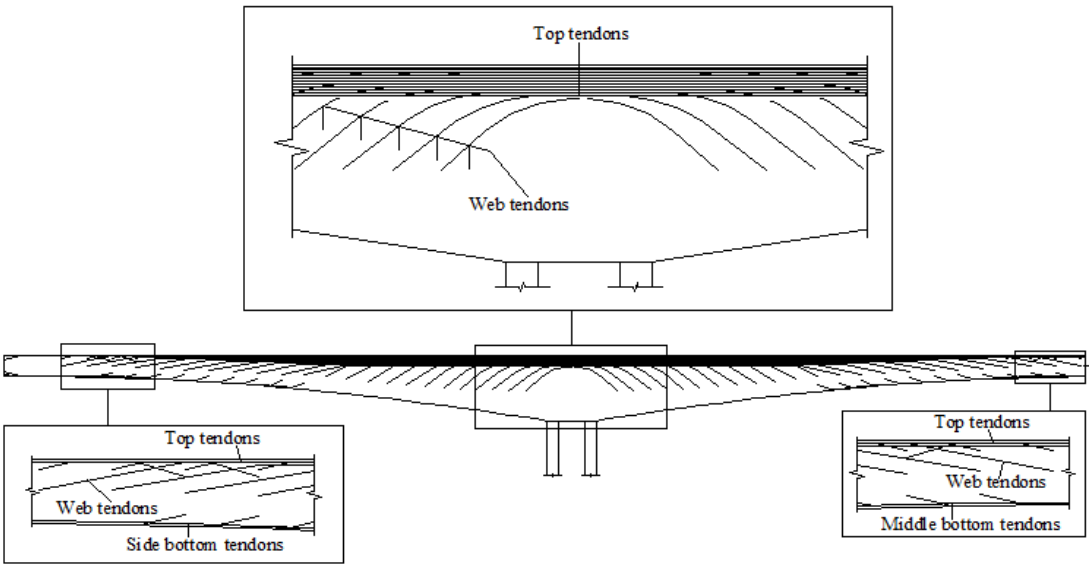

Fig. 5 Arrangement of prestressing tendons in PC bridge

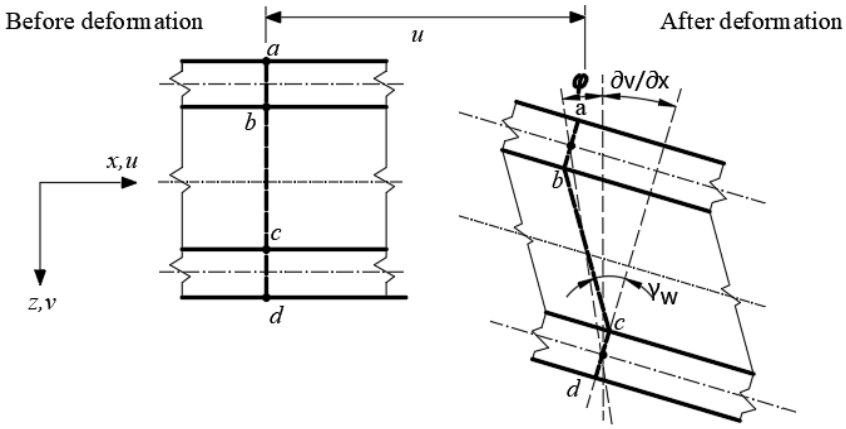

(a) Deformation

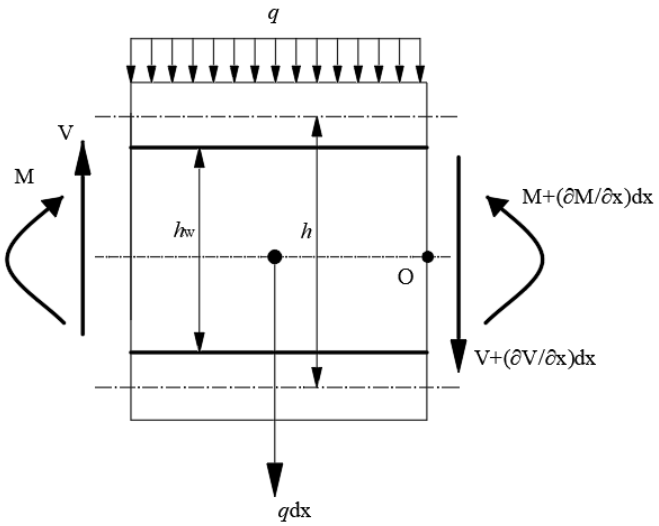

(b) Forces equilibrium

Fig. 6 Description of sandwich beam element

webbing needed to be considered in their model because there was an uncoordinated deformation between the top and bottom flanges and the web plates. Further studies by Fujioka and Kakuta (2005) and Shiratani *et al*. (2002) have revealed that the axial stiffness of corrugated steel webbing is much larger than has typically been assumed, sometimes by as much as 25% above the value predicted by conventional analysis where the stiffness of the webbing has been ignored. All in all, the assumption that there is negligible axial stiffness in corrugated webbing is, at the very least, conservative. A sandwich beam model originally proposed by Chen *et al*. (2016) has therefore been introduced in this study. A typical beam segment of a girder with corrugated steel webbing is shown in Fig. 6. The bending deflection, and shear deflection, need to be superimposed to take into account their interaction. If the transverse shear force acting on the bridge varies with the abscissa x, there will be additional curvature, together with a secondary shear force, and a bending moment, causing a concentration of stress in the concrete flanges. Consideration of equilibrium and compatibility in this case will give

$$V_1'' - \alpha^2 V_1 = -\alpha^2 V \tag{1}$$

$$\alpha^2 = \frac{\beta^2 S_w}{B_f} \bullet \frac{B}{B_g} \tag{2}$$

$$\beta = \frac{h}{h_w} \tag{3}$$

$$B = B_f + B_g \tag{4}$$

where, V_1 = the primary shear force; V = the total shear force; S_w = the shear rigidity of the corrugated webs; B_f = the sum of the local flexural rigidity of the flanges around their respective centroidal axes; and B_g = the global flexural rigidity of the flanges around the centroidal axis of the entire beam section, assuming uniform stress in each flange.

The two conceptual schemes of a PC bridge with corrugated steel webbing and a traditional PC bridge were simulated using sandwich beam elements. A traditional Euler-Bernoulli beam element was introduced to simulate the piers and a compressive-only truss element was adopted

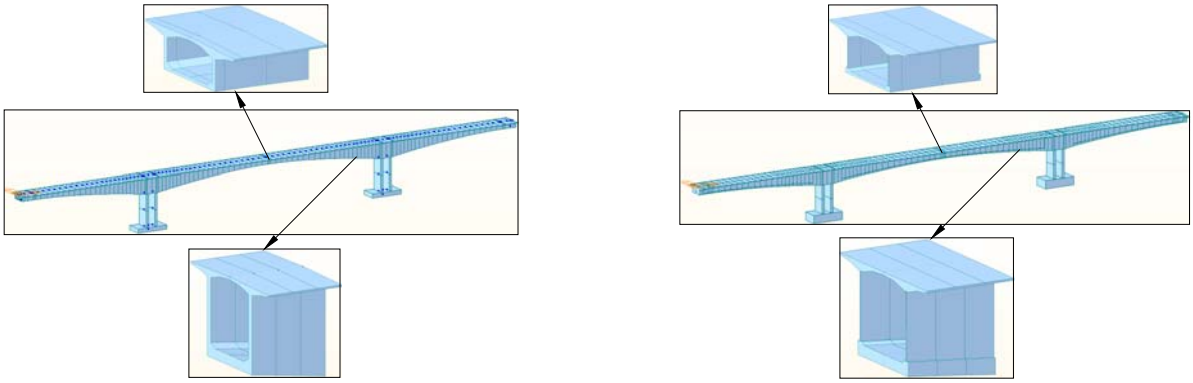

(a) Type I: PC bridge (b) Type II: PC bridge with corrugated web

Fig. 7 Finite element models

to discretize the prestressing tendons. The finite element models are shown in Fig. 7. As the foundations were enough strong for the pile, the boundary was set to be fixed at the bottom of the pile and the pile-soil coupling effect was ignored. In order to make a meaningful comparison, the model details and construction stages of both bridges were considered to be almost the same apart from the section dimensions and quantity of prestressing tendons. For convenience, from now on the traditional PC bridge will be referred to as Type-I and the PC bridge with corrugated steel webbing will be referred to as Type-II.

4.2 Creep model

Even though it has been proved that the existing empirical creep prediction models can result in a gross underestimation of multi-decade creep deflections (Bazant *et al*. 2011), they are still often directly applied to real projects by engineers. At present, several empirical creep models are used to simulate long-term behavior using finite-element methods. These include: the American Concrete Institute (ACI) 209 model (ACI Committee 209 2011); the B3 model (Bazant and Baweja 1995); the Comite Euro-international du Beton – Federation Internationale de la Precontrainte (CEB-FIP) model (1978, 1990); the GL2000 model (Gardner and Lockman 2001); and the American Association of State Highway and Transportation Officials Load and Resistance Factor Design (AASHTO LRFD) model (AASHTO 2010). These creep models can be roughly divided into two categories: asymptotic and logarithmic. The first of these covers most of the creep models presented in design codes, recommendations, and standards. These asymptotic models predict long-term ultimate creep strains that are approached asymptotically over time. This category includes the AASHTO LRFD model (AASHTO 2010), the 1978 and 1990 CEB-FIP model codes (CEB-FIP 1978, 1990), and the ACI 209 (1992) model. The logarithmic models, such as the B3 model (Bazant and Baweja 1995), use a notion of long-term creep strains tending to approximate linearly as a logarithm of time, instead of predicting ultimate creep strains. Although the mathematical form of the GL2000 creep model (Gardner and Lockman 2001) implies an asymptotic creep strain, for typical concrete properties and load durations less than thousands of years the asymptotic behavior is never observed. For normal structural life spans up to 150 years, the GL2000 creep model behaves much like a logarithmic creep model and will consequently be classified as such for the purposes of this study. Unlike creep, most shrinkage models progress asymptotically to an ultimate shrinkage strain. Physically, this is justified because the mechanisms that induce shrinkage are limited by the movement or chemical processes of water (Neville 1996). When the system has reached an equilibrium state, the shrinkage will cease. Although limited, the AASHTO, ACI 209, CEB-FIP (1990) and GL2000 models were chosen to analyze the time-dependent behavior of the two types of bridge discussed in this paper.

5. Results and discussion

5.1 Creep coefficient

The input characteristics required by all of the creep models are: the average compressive strength of the concrete; the environmental relative humidity; and the effective cross-sectional thickness. In addition, some of the model use the water-cement ratio (w/c), the specific cement content c, and the aggregate-cement ratio (a/c) as input. If these additional input values are unknown, the recommended default values are used. It was assumed for the various creep models that the designed concrete strength was 48 MPa at 28 days. The average effective cross-sectional thickness was taken to be he = 865 mm, with an environmental humidity of 75%. For the other parameters, it was assumed that w = 207.92 kg/m^3, w/c = 0.46, a/c = 3.73 and γ = 2405 kg/m^3, with it being ordinary Portland cement and moist-cured concrete. The age of the concrete at loading was assumed to be t_0 = 7 days for the CEB-FIP, ACI, and AASHTO models and the age of the concrete at the beginning of shrinkage was assumed to be t_c = 7 days for the GL2000 model. The creep coefficient for four of the creep models - CEB-FIP (1990), ACI209R-92, AASHTO, and GL2000 - are shown in Fig. 8 and Table 1. The creep coefficient curves for the CEB-FIP (1990), ACI209R-92

and AASHTO models show an asymptotic behavior that varies over time, while the curve for the GL2000 model shows a sustained increasing over time. Up to 180 days, the creep coefficients obtained by the ASSHTO code more or less agree with those obtained by the ACI209 and CEB-FIP codes. After six months, gaps begin to appear between each model for the creep coefficient. The creep coefficient obtained by the ASSHTO code is significantly smaller than it is for the other codes at the same given time. The maximum ASSHTO creep coefficient is less than 1.0. The creep coefficient curves for the ACI and CEB-FIP codes are similar due to the similarity between their specifications. Beyond 1600 days, the creep coefficient for the CEB-FIP (1990) model and the ACI209R-92 model begins to stabilize, with a maximum value of between 1.5 and 2.0. The maximum creep coefficient for the GL2000 model, meanwhile, exceeds 2.0.

5.2 Longitudinal Deflection

Fig. 9 shows a comparison between the longitudinal deflections at the expansion joints for the Type-I and Type-II bridges. The adjusted age of zero was assumed to correspond to the date when the construction was completed. The longitudinal deflection in the horizontal direction shows that both the instantaneous and long-term deflection for the PC bridge with corrugated steel webbing was smaller than it was for the conventional PC bridge. It can be seen that the longitudinal deformation values at the expansion joints based on the CEB-FIP (1990), ACI 209 (2011) and GL2000 models show a certain degree of consistency, whilst the values for the AASHTO model are evidently different. The reason for this is that the creep coefficient for the AASHTO code is significantly smaller than it is for the other three. A comparison between the

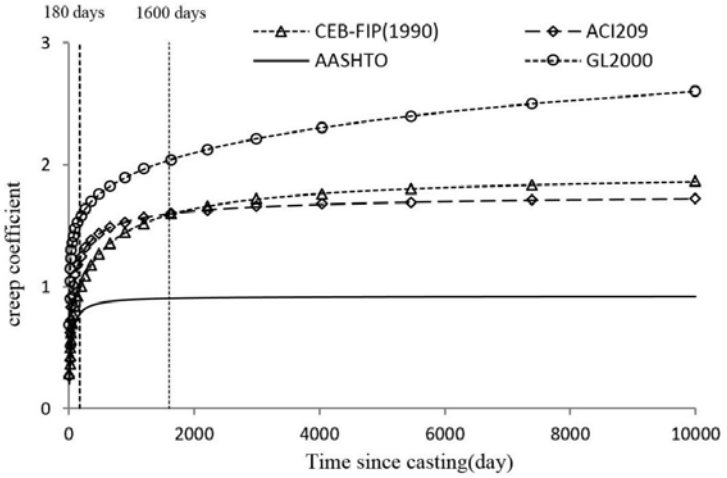

Fig. 8 Results of creep coefficient

Table 1 Creep coefficient results at typical testing time

d (day)	CEB-FIP(1990)	ACI209	AASHTO	GL2000	d (day)	CEB-FIP(1990)
7	0.284	0.263	0.205	0.692	7	0.284
14	0.367	0.400	0.257	0.906	14	0.367
28	0.564	0.729	0.452	1.231	28	0.564
180	1.006	1.252	0.789	1.582	180	1.006
360	1.179	1.382	0.844	1.697	360	1.179

Table 2 Longitudinal deflection at expansion joint (unit: mm)

Time (day)	CEB-FIP			ACI		AASHTO			GL2000			
	Type I	Type II	Ratio	Type I		Type I	Type II	Ratio	Type I		Type I	Type II
14	7.15	1.31	82%	9.70	14	7.15	1.31	82%	9.70	14	7.15	1.31
28	9.32	1.47	84%	20.06	28	9.32	1.47	84%	20.06	28	9.32	1.47
365	27.24	3.10	89%	29.91	365	27.24	3.10	89%	29.91	365	27.24	3.10
3650	46.69	5.55	88%	40.43	3650	46.69	5.55	88%	40.43	3650	46.69	5.55
Average			86%		average			86%		average		

*Note: Type I-----PC bridge; Type II-----PC bridge with corrugated steel web; ratio = (I-II) / I×100%

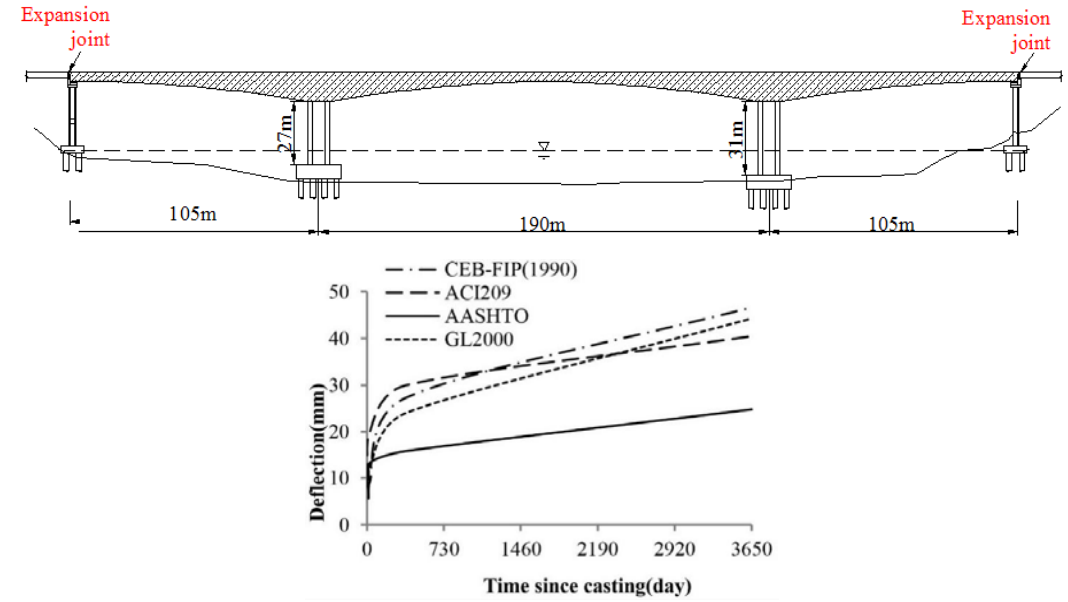

(a)Type I

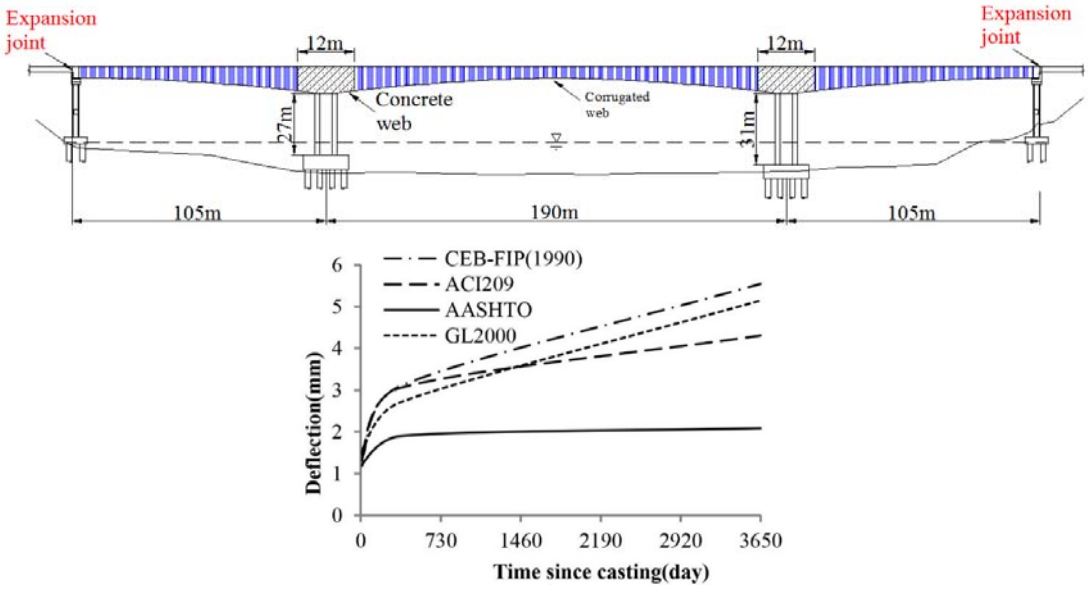

(b)Type II

Fig. 9 Longitudinal deflection results at expansion joint

Type I and Type II bridges for the long-term longitudinal deflection after a typical period is shown in Table 2. It can be seen from the Table that the longitudinal deformation at the expansion joints for the Type I bridge was less than it was for the Type II bridge by 86%(CEB-FIP), 89%(ACI), 87%(AASHTO) and 87%(GL2000), respectively.

5.3 Vertical deflection

Some investigations have suggested that the vertical deflection of concrete bridges is still increasing after periods of between 20 and 50 years (Bazant *et al*. 2011). This is contrary to the common consensus, which suggests that the long-term vertical deflection can be ignored after 6 months. In view of this, predictions for 14 days, 28 days, 1 year and 10 years after the time of completion were carried out to examine how the vertical deflection varied over time between the Type I and Type II bridges. The results are shown in Fig. 10. It can be seen that the shape of the time-dependent deflection displays a similar trend for both types of bridge. The absolute deflection in the vertical direction for the mid-span is greater than it is for the side-span, with the maximum deflection being generated in the mid-span. Initially (for the periods up to 28 days), the curves for all four creep models for the Type I bridge are more or less coincident. Apart from in the case of the AASHTO model, the long-term deflection continues to grow for the periods up to 1 year and 10 years. For the Type II bridge, the values calculated by the different models are in close agreement. The long-term vertical deflection of the Type II bridge for all four creep models remains constant and the values at the same points in time are systematically less than they are for

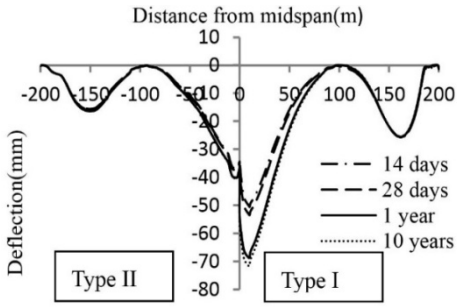

(a) ASSHTO

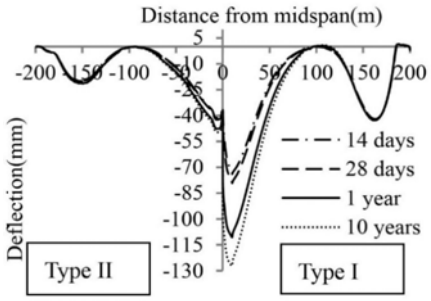

(b) ACI

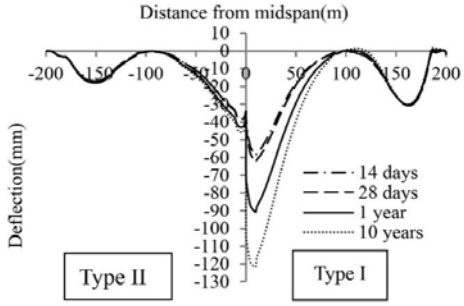

(c) CEB-FIP

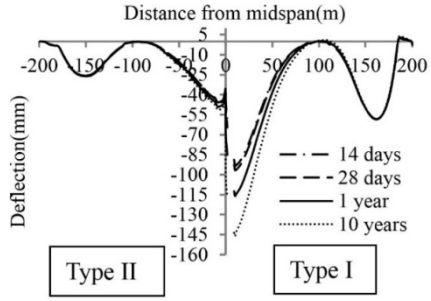

(d) GL2000

Fig. 10 Vertical deflection results at different period

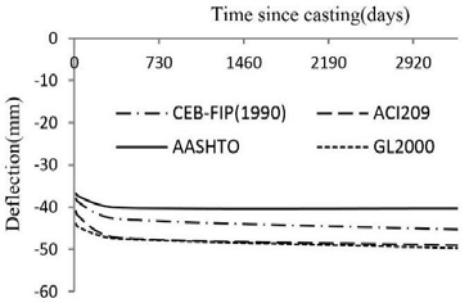

(a) Type II

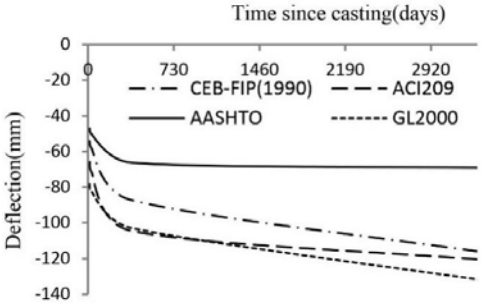

(b) Type I

Fig. 11 Long-term deflection at middle section of mid-spa

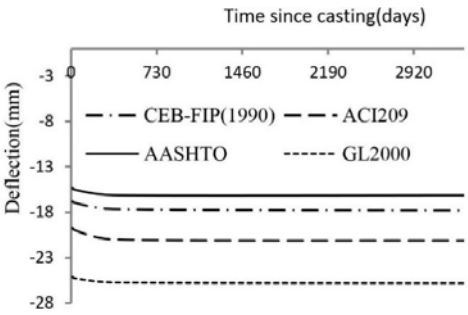

(a) Type II

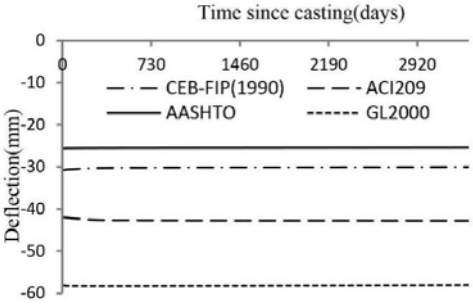

(b) Type I

Fig.12 Long-term deflection at middle section of side-span

the Type II bridge, by a factor of up to 50%. It can also be seen from Fig. 10 that the deflection calculated by the four creep models displays certain differences for the middle part of the span in both of the bridges, while the side span results remain consistent.

Figs. 11-12 show the results of the long-term deflection for the middle section of the mid-span and the side-spans, respectively. The effect of the creep on the middle span is more significant than it is on the side span, for both bridges. For specific models, the long-term deflection of the middle

Table 3 The maximum deflection value of the side-span

Time (day)	CEB-FIP			ACI			AASHTO			GL2000		
	Type I	Type II	Ratio	Type I	Type II	Ratio	Type I	Type II	Ratio	Type I	Type II	Ratio
14	-30.79	-16.78	46%	-42.00	-19.69	53%	-25.58	-15.37	40%	-58.10	-25.10	57%
28	-30.73	-16.92	45%	-42.06	-19.92	53%	-25.55	-15.50	39%	-58.21	-25.24	57%
365	-30.24	-17.65	42%	-42.69	-20.98	51%	-25.49	-16.11	37%	-58.29	-25.72	56%
3650	-30.01	-17.82	41%	-42.80	-21.12	51%	-25.35	-16.12	36%	-58.00	-25.82	55%
Average			86%			89%			87%			87%

Table 4 The maximum deflection value of the side-span

Time (day)	CEB-FIP			ACI			AASHTO			GL2000		
	Type I	Type II	Ratio	Type I	Type II	Ratio	Type I	Type II	Ratio	Type I	Type II	Ratio
14	-54.09	-38.02	30%	-65.71	-40.92	38%	-47.24	-36.77	22%	-78.44	-43.97	44%
28	-57.97	-38.69	33%	-71.44	-41.97	41%	-50.22	-37.34	26%	-82.26	-44.65	46%
365	-87.11	-42.79	51%	-104.42	-47.23	55%	-66.13	-40.14	39%	-102.83	-47.42	54%
3650	-119.10	-45.56	62%	-121.96	-49.20	60%	-69.19	-40.35	42%	-134.74	-49.91	63%
Average			44%			48%			32%			52%

section of the mid-span increases over time, while that of the side-span keeps more or less constant. The results also show that the long-term deflection of the mid-span is greater than it is for the side-span. Here, the deflection of the Type I bridge is between 2.5 and 3.0 times that of the Type II bridge. In Fig. 11, it can be seen that the values for the ACI 209 and GL2000 models are in close agreement but distinct from those for the AASHTO and CEB-FIP models. At the same moment in time, the AASHTO model presents its minimum deflection while both the ACI 209 and GL2000 models present their maximum deflection and the CEB-FIP model indicates a value in-between. In Fig. 12, the long-term deflection of the side-span for both bridges shows little change over time in any of the models.

The maximum deflections at the middle of the side-span and mid-span are shown in Tables 3-4, covering periods of 14 days, 28 days, 1 year and 10 years. The results obtained by all four models illustrate that the maximum deflection of the Type II bridge is smaller than that of the Type I bridge, in both the side-span and the mid-span. The average ratio of reduction in the maximum deflection between the Type II and Type I bridges for the side-span is about 43%(CEB-FIP), 52%(ACI), 38% (AASHTO) and 56%(GL2000), respectively. The corresponding values for the mid-span are 44%(CEB-FIP), 48%(ACI), 32% (AASHTO) and 52%(GL2000), respectively. Though the weight of the Type II bridge is less than that of the Type I bridge, the long-term deflection of the Type II is always smaller than that of the Type I, especially in the mid-span during the later stages of loading. The reason for this is that the energy exchange between a concrete web box girder and the environment is more significant than it is in the case of a corrugated steel web box girder. So, under higher compressive stress, the growth ratio for the long-term deflection of a Type I bridge is greater than that of a Type II bridge. This suggests that the long-term deflection of a concrete web box girder will be more influenced by concrete creep. For the side span, the deflection values for both types of bridge only slightly increased.

5.4 Prestress loss analysis

As may be recalled from above, there were both internal and external prestressing tendons in the Type II bridge while there were only internal prestressing tendons in the Type I. In the Type II, the internal prestressing tendons were assumed to be able to bear the main reaction to dead and live loads while the external prestressing tendons were set to adjust the pre-camber to meet the bridge's requirements during the whole of its serving life. The tension control stress of the internal tendons was 1395 MPa and, for the external tendons, it was set to 1160 MPa.

The average prestressing loss of the Type I bridge is given in Fig. 13. After a short period, the prestressing loss obtained by all four models reached about 15% and this continued to increase over time. The rate of increase for the CEB-FIP, ACI 209 and GL2000 models remained consistent. However, it is striking that in the AASHTO model the prestressing loss showed almost no growth after it had reached the maximum instantaneous elastic loss. The results also show that variations in the prestressing loss

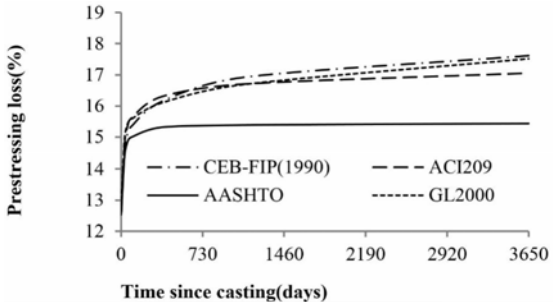

Fig. 13 Prstressing loss result (Type I)

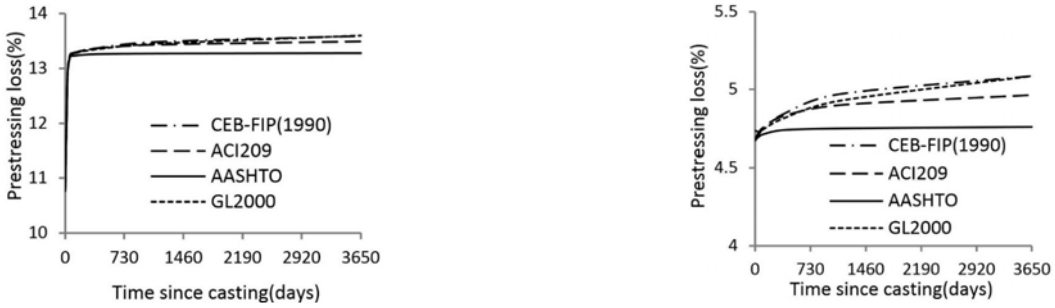

(a) Interior (b) Exterior

Fig. 14 Prstressing loss results (Type II

were similar across the CEB-FIP, ACI and GL2000 models. The initial prestress loss calculated by the CEB-FIP, ACI and GL2000 models was about 15%, increasing over time to a maximum of about 18%. The prestressing loss according to the AASHTO model started at about 15% and remained more or less the same.

The prestressing loss for the internal and external tendons of the Type II bridge is shown in Fig. 14. The elastic loss of the internal prestressing tendons was about 13% and about 4.8% for the external ones. Over the passage of time, the prestressing loss of the internal tendons showed almost no further growth and even for the external tendons the growth remained very small. The maximum prestressing loss value for the external tendons was about 5%. As with the Type I bridge, it was found that the AASHTO model presented a smaller result than the other three models for both the internal and external prestressing tendons. Taking Figs. 13 and 14 together, it can be seen that the CEB-FIP, ACI 209 and GL2000 models have highly coincident curves for the trends in prestressing loss and a higher absolute value than the results from the AASHTO model. Note, also, that the prestressing loss for the Type II bridge was smaller than it was for the Type I.

5.5 Stress results

In order to analyze their stress status, the stress experienced by the two types of bridges was compared. As the long-term behavior of steel webbing under common working stress is virtually time independent it can be ignored, so the results are focused on the concrete (Jiang *et al*. 2015, Chen *et al*. 2015). In order to make a comparison under one specific condition, a combined Dead Load (DL) / Live Load (LL) case of DL+0.5LL was selected to carry out the calculations. The long-term stress on the upper flanges at the middle of the mid-span is shown in Fig. 15, over a period from the beginning to 10 years after casting. It can be seen that the stress for the Type I bridge calculated according to the different creep models varied greatly over time. This coincides with the findings of previous research (e.g., Chen *et al*. 2017). The stress for the Type II bridge remained largely constant over time. The absolute stress value was about 6.0 MPa for the Type I bridge but, for the Type II bridge, it increased over time to 16 MPa (GL2000) after 10 years. The reason for this is that the concrete flanges of the Type II bridge work like a pure slab because of a weakness in the axial stiffness of corrugated steel webs. The same phenomenon was observed by Chen *et al*. (2015, 2017) and Chen *et al*. (2017). Higher stress induces higher long-term vertical deflection, meaning that the long-term deflection of a Type II bridge will be more serious than that of a Type I bridge. The normal stress distribution for the interior piers for the two types of bridge is shown in Fig. 16. The results show that, although the stress for both bridges increases over time, the absolute values at the same age are roughly equivalent according to the same models. This is

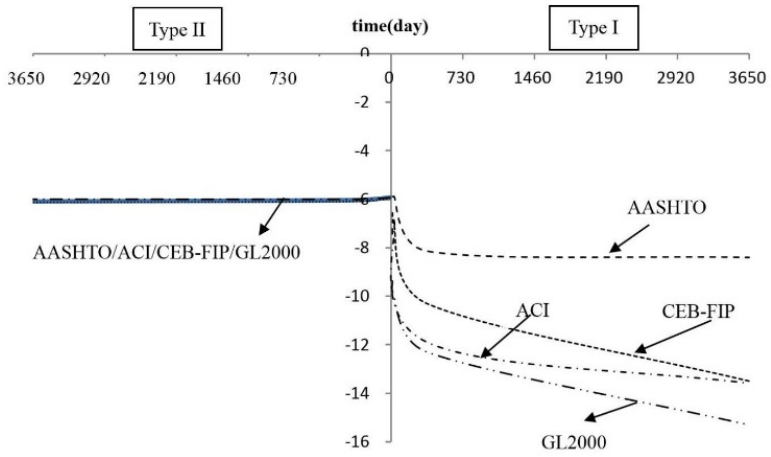

Fig. 15 Stress result of top flange at the middle section

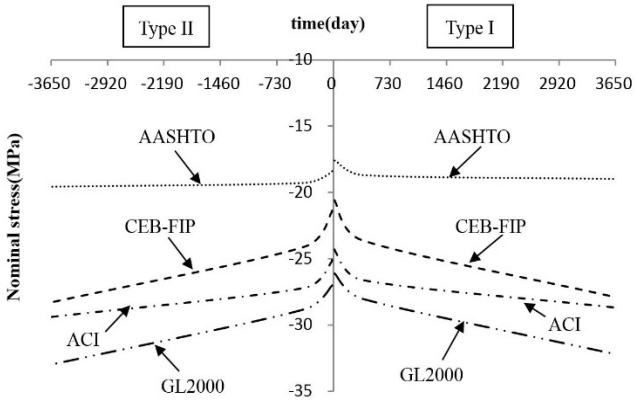

Fig. 16 Stress result of top flange at the interior pier

because the section near the interior pier is very similar in both bridges. Figs. 15 and 16 together reveal that the stress value for the interior pier is larger than that of the mid-span.

5.6 Parameters analysis

For continuous beam bridge, because the relationship between girder height and span is often satisfied with empirical formula, thus, the ratio of side to middle span is one of the main factors affecting the long-term behavior. Besides, the control prestressing tension stress is another essential factor affecting the long-term deformation of bridges. Therefore, the mid-side span ratio and control prestressing tension stress are chosen as the basic variables for parameter analysis. Considering comparison, the calculation time is uniformly set at 1000 days. The long-term deformation at mid-span section is shown as Fig. 17. It can be seen that with the increase of the side-to-mid span ratio, the deflection direction at mid-span section gradually changes from the downward to upward. When the ratio of side-to-mid span is about equal to 0.55, the deflection at mid-span section is the smallest nearly zero. When the ratio of side-to-mid span is less than 0.55, the long-term deflection at mid-span section is downward. Especially when the ratio is smaller, the absolute value of long-term deflection is much larger and may lead to structural insecurity, which is consistent with the conclusions of Bazant *et al*. (2011). When the ratio of side-to-mid span is

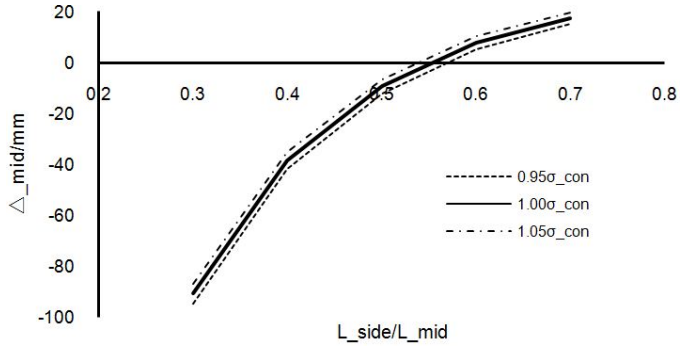

Fig. 17 Long-term deflection at mid-span section influenced by span ratio

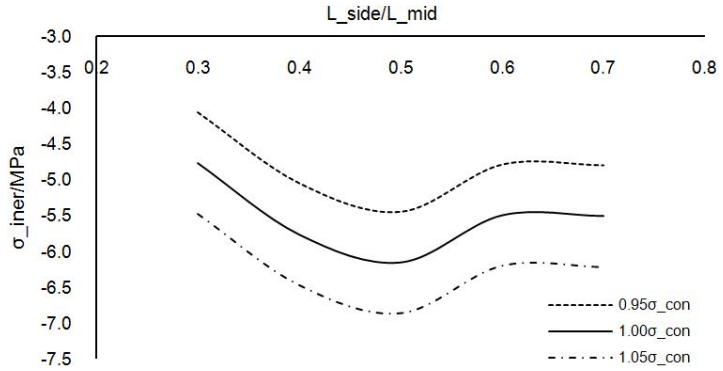

Fig. 18 Stress of top flange at inner-pier section influenced by span ratio

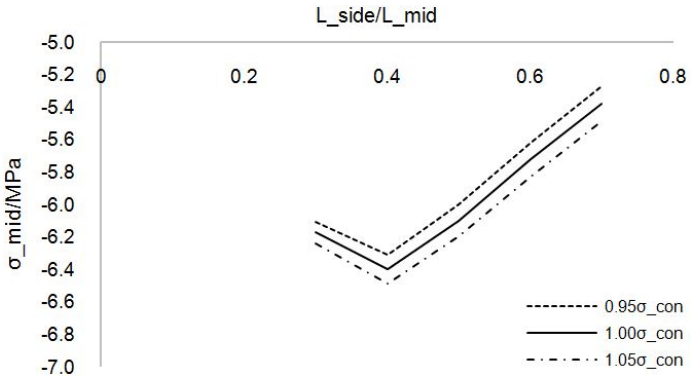

Fig. 19 Stress of top flange at mid-span section influenced by span ratio

greater than 0.55, the upward deflection at midspan increases by the side-to-mid span ratio. The concrete stress of top flange at inner-pier section is shown as Fig. 18. It can be seen that the absolute value of compressive stress of flange concrete increases first and then decreases with the side-to-mid span ratio, reaching the maximum at 0.55. The concrete stress of top flange at mid-span section is shown as Fig. 19. It also shows the same rule as stress of top flange at inner-pier, which is the absolute value of concrete stress increase first and then decreases with the side-to-mid span, it reaches its maximum result at about 0.4. It is worth mentioning that the effect of control prestressing tension stress on the results is consistent.

6. Analysis of the factors influencing the creep effect

The Type II bridge was impacted by many factors, including the loading age, the environmental relative humidity, and the strength of the concrete. Most of the basic creep models take the volume/surface ratio to be the most influential parameter, apart from the CEB-FIP (1990) model, which replaces it with effective thickness. In view of the limits of a single publication, this article can only discuss the loading age and environmental relative humidity by taking the AASHTO and CEB-FIP creep models as examples to simulate the long-term behavior. From the preceding analysis, concrete creep has a major impact on the long-term deflection, but less of an influence on the prestress loss and normal stress. Thus, this section only analyzes the deflection distribution according to the different factors that can affect creep. In particular, when concrete is subjected to sustained stress, it undergoes deformation that increases over time. In order to compare the results meaningfully, the construction stages and material properties are strictly aligned with the real project.

6.1 Loading age

Ages of 5 days, 7 days, 10 days, 14 days, 28 days and 3650 days were selected to compare the impact of loading age, while all the other parameters were kept constant. The long-term deflection according to loading age for the ASSHTO and CEB-FIP models is shown in Fig. 20. It can be seen that the deflection of the Type II bridge increased over time, with the loading age having some degree of influence. However, it has almost no impact on the Type II bridge. In relation to this, the absolute maximum value of long-term deflection for the Type II bridge is much smaller than it is for the Type I bridge.

The typical long-term deflection values considering the influence of loading age are listed in Tables 5 and 6. For the same loading age, the long-term deflection of the Type II bridge was between 50% and 70% of that of the Type I bridge, with the Type II bridge not being sensitive to loading age. Variations in the concrete loading age have little influence on the creep coefficient. The maximum

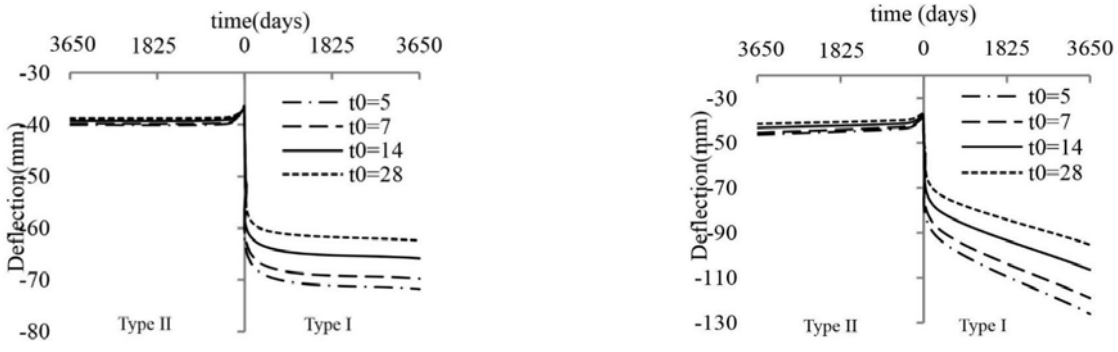

AASHTO model CEB-FIP model

Fig. 20 Long-term deflection at mid-span section influenced by loading age

Table 5 Long-term deflection under different loading age in CEB-FIP (1990) model (unit: mm)

Time (day)	t0 = 5			t0 = 7			t0 = 14			t0 = 28		
	Type I	Type II	Ratio	Type I	Type II	Ratio	Type I	Type II	Ratio	Type I	Type II	Ratio
14	-59.7	-46.3	0.78	-57.4	-45.3	0.79	-53.2	-43.2	0.81	-49.4	-41.5	0.84
28	-63.6	-43.4	0.68	-61.1	-42.6	0.70	-56.4	-41.1	0.73	-52.3	-39.7	0.76
365	-93.2	-39.2	0.42	-88.8	-38.7	0.44	-80.4	-37.7	0.47	-73.1	-36.8	0.50
3650	-126.0	-38.5	0.31	-119.1	-38.0	0.32	-106.3	-37.1	0.35	-95.2	-36.3	0.38
Average			0.55			0.56			0.59			0.62

6.2 Environmental relative humidity

Table 6 Long-term deflection under different loading age in AASHTO model (unit: mm)

Time (day)	t0 = 5			t0 = 7			t0 = 14			t0 = 28		
	Type I	Type II	Ratio	Type I	Type II	Ratio	Type I	Type II	Ratio	Type I	Type II	Ratio
14	-50.0	-36.5	0.73	-49.0	-36.4	0.74	-49.0	-36.5	0.74	-49.7	-36.8	0.74
28	-53.0	-37.1	0.7	-51.8	-36.9	0.71	-51.1	-36.9	0.72	-51.2	-37.0	0.72
365	-68.8	-39.9	0.58	-67.0	-39.6	0.59	-63.4	-39.0	0.62	-60.2	-38.6	0.64
3650	-71.8	-40.1	0.56	-69.8	-39.8	0.57	-65.9	-39.2	0.59	-62.4	-38.8	0.62
Average			0.60			0.70			0.70			0.70

* Type I = PC bridge; Type II = PC bridge with corrugated steel web. Ratio = Type II/Type I

creep coefficient in the AASHTO model was approaching 1 and variations in the deflection of the Type II bridge's mid-span under different loading ages was within 10 mm. For the AASHTO model, the long-term deflection of the Type II changed from 40.1 mm to 38.8 mm as the loading age changed from t0 = 5 to t0 = 28. The corresponding variation for the Type I varied from 71.8 mm to 62.4 mm at an age of 3650 days. For the CEB-FIP model, the long-term deflection of the Type II changed from 38.5 mm to 36.3 mm as the loading age changed from t0 = 5 to t0 = 28. The corresponding variation for the Type I varied from 126.0 mm to 95.2 mm at an age of 3650 days. In both models, the rate of change for the Type I bridge was much bigger than for the Type II. All in all, the loading age seems to play a minor role in the long-term deflection of Type II bridges and can be ignored. This means that long-span PC bridges with corrugated steel webbing are viable for widespread adoption when using a segmental cantilever construction approach because the casting period for the segments never exceeds 10 days.

In order to study the influence of environmental relative humidity, the relative humidity was set variously to 55%, 65%, 75% and 85%, with a loading age of 7 days for both models. The long-term deflection taking into account the influence of environmental relative humidity is shown for both models in Fig. 21. The same phenomenon as before was found, i.e. the deflection for the Type I bridge showed evident variation over time in both models, while, for the Type II bridge, it remained almost constant. Additionally, the long-term deflection of the Type II bridge in relation to environmental relative humidity was smaller than that it was for the Type I bridge. The typical long-term deflections for an environmental relative humidity of 40%, 65%, 75% and 85% are shown in Tables 7 and 8. At the same environmental relative humidity, the long-term deflection of the Type II bridge was between 51% and 70% of that of the Type I bridge, with the Type II bridge not showing any significant sensitivity to environmental relative humidity. When the environmental relative humidity changed from 85% to 55%, the deflection value for the mid-section in the

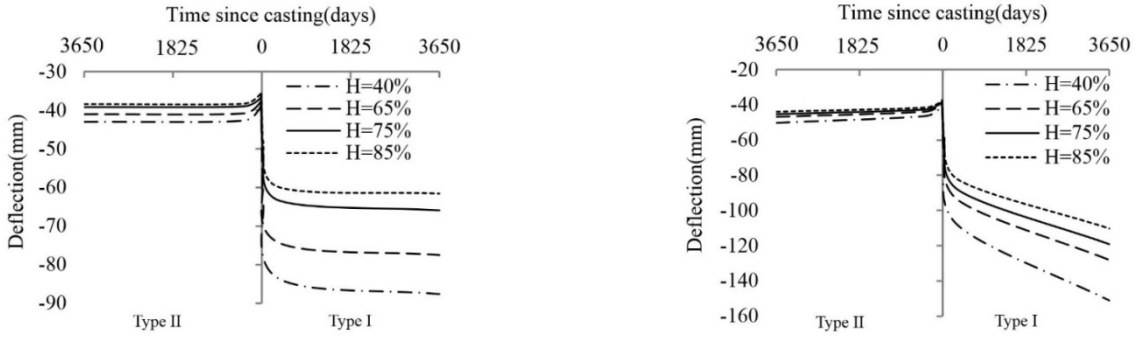

AASHTO model CEB-FIP model

Fig. 21 Long-term deflection at mid-span section influenced by relative humidity

Table 7 Long-term deflection under environmental relative humidity in AASHTO model (unit: mm)

Time (day)	H = 40%			H = 65%			H = 75%			H = 85%		
	Type I	Type II	Ratio	Type I	Type II	Ratio	Type I	Type II	Ratio	Type I	Type II	Ratio
14	-60.3	-43.0	0.71	-54.9	-41.0	0.75	-49.0	-39.2	0.80	-45.5	-38.4	0.84
28	-64.0	-42.7	0.67	-57.9	-40.8	0.70	-51.1	-39.0	0.76	-48.1	-38.3	0.80
365	-83.7	-39.2	0.47	-74.4	-37.9	0.51	-63.4	-36.9	0.58	-60.0	-35.8	0.60
3650	-87.6	-38.5	0.44	-77.5	-37.3	0.48	-65.9	-36.5	0.55	-61.6	-35.3	0.57
Average			0.57			0.61			0.67			0.70

Table 8 Long-term deflection under environmental relative humidity in CEB-FIP model (unit: mm)

Time (day)	H = 40%			H = 65%			H = 75%			H = 85%		
	Type I	Type II	Ratio	Type I	Type II	Ratio	Type I	Type II	Ratio	Type I	Type II	Ratio
14	-67.7	-50.3	0.74	-60.3	-46.7	0.77	-57.4	-45.3	0.79	-54.5	-43.9	0.81
28	-72.6	-46.4	0.64	-64.4	-43.7	0.68	-61.1	-42.6	0.70	-57.9	-41.5	0.72
365	-109.2	-41.1	0.38	-94.6	-39.4	0.42	-88.8	-38.7	0.44	-83.0	-38.0	0.46
3650	-151.1	-40.3	0.27	-128.1	-38.7	0.30	-119.1	-38.0	0.32	-110.3	-37.4	0.34
Average			0.51			0.54			0.56			0.58

mid-span of the Type I bridge increased by nearly 40 mm in the CEB-FIP (1990) model. However, for the Type II, the same measure of change was only about 3 mm.

7. Conclusions

In this study, a comparison was undertaken between the long-term behavior of a conventional PC bridge and one with corrugated steel webbing. This led to the following observations:

- The long-term deformation of a PC bridge with corrugated steel webbing is significantly smaller than it is for a conventional PC bridge, in terms of both the horizontal deformation and the deflection at the middle of the mid-span. It can be concluded from this that, when it comes to establishing bridge specifications, pre-cambering will not be needed for PC bridges with corrugated steel webbing, but will still be needed for conventional PC bridges.
- As a result of the "accordion effect" in corrugated webs, the stress distribution at the top and bottom flanges of a PC bridge with corrugated steel webbing is more uniform than that of conventional PC bridge. The stress in PC bridges with corrugated steel webbing remains nearly constant throughout its serving life, while, for conventional PC bridges, it increases over time.
- The top and bottom concrete flanges in Type II bridges behave like thin plates because of the relatively weak axial stiffness of corrugated steel webs, so, the prestressing tendons need to supply sufficient effective prestress. Thus, the prestressing loss in both types of bridge is similar over the longer term.
- The long-term deformation value of the PC bridge with corrugated steel webbing is small when the side-to-mid span ratio is about 0.5. It is suggested that the design value should be between 0.4 and 0.6.
- Relative to conventional PC bridges, PC bridges with corrugated steel webbing are not sensitive to loading age and environmental humidity.

In view of the above findings, we would conclude that further experimental research and the development of health monitoring systems are required to further progress our understanding of the long-term behavior of PC bridges with corrugated steel webbing.

References

AASHTO (2010), AASHTO LRFD bridge design specifications; (5th Edition), Washington, DC, USA.

ACI Committee 209 (2011), ACI2092R-08 Prediction of creep, shrinkage, and temperature effects in concrete structure; American Concrete Institute, Detroit, MI, USA.

Bažant, Z.P. and Baweja, S. (1995), "Creep and shrinkage prediction model for analysis and design of concrete structures–model B3", *Mater. Struct.*, **28**(6), 357-365.

Bažant, Z.P., Hubler, M.H. and Yu, Q. (2011), "Pervasiveness of excessive deflections of segmental bridges: wake-up call for creep", *ACI Struct. J.*, **108**(6), 766-774.

Bažant, Z.P., Qiang, Y. and Li, G.H. (2012a), "Excessive long-time deflections of prestressed box girders. I: record-span bridge in Palau and other paradigms", *J. Struct. Eng.*, **138**(6), 676-686.

Bažant, Z.P., Yu, Q. and Li, G.H. (2012b), "Excessive long-time deflections of prestressed box girders. II: numerical analysis and lessons learned", *J. Struct. Eng.*, **138**(6), 687-696.

CEB-FIP (1978), CEB-FIP 1978 model code; *Comite Euro-International duBeton-Federation International dela Precontrainte*, Thomas Telford, London, UK.

CEB-FIP (1990), CEB-FIP 1990 model code; *Comite Euro-International duBeton-Federation International dela Precontrainte*, Thomas Telford, London, UK.

Chan, C.L., Khalid, Y.A., Sahari, B.B. and Hamouda, A. (2002), "Finite element analysis of corrugated web beams under bending", *J. Constr. Steel Res.*, **58**(11), 1391-1406.

Chen, X.C., Au, F.T.K., Bai, Z.Z., Li, Z.H. and Jiang, R.J. (2015), "Flexural ductility of reinforced and prestressed concrete sections with corrugated steel webs", *Comput. Concrete*, *Int. J.*, **16**(4), 625-642.

Chen, X.C., Li, Z.H., Au, F.T.K. and Jiang, R.J. (2016), "Flexural vibration of prestressed concrete bridges with corrugated steel webs", *Int. J. Struct. Stab. Dyn.*, **16**(10), 1750030-1-30.

Chen, X.C., Pandey, M., Bai, Z.Z. and Au, F.T.K. (2017), "Long-term behavior of prestressed concrete bridges with corrugated steel webs", *J. Bridge Eng.*, *ASCE*, **22**(8), 04017040-1-5.

Cheyrezy, M. and Combault, J. (1990), "Composite bridges with corrugated steel webs—Achievements and prospects", *IABSE Symposium*: *Mixed Structures including New Materials*, *IABSE*, Zurich, Switzerland, pp. 479-484.

Combault, J. (1988), "The Maupré Viaduct near Charolles, France", *Proceedings of American Institute of Steel Construction National Steel Construction Conference*, Miami Beach, FL, USA, Volume 12, pp. 1-22.

Elamary, A., Ahmed, M.M. and Mohmoud, A.M. (2017), "Flexural behaviour and capacity of reinforced concrete–steel composite beams with corrugated web and top steel flange", *Eng. Struct.*, **135**, 136-148.

Elgaaly, M., Seshadri, A. and Hamilton, R.W. (1997), "Bending strength of steel beams with corrugated webs", *J. Struct. Eng.*, *ASCE*, **123**(6), 772-782.

Fujioka, A. and Kakuta, T. (2005), "Application of the corrugated steel webs to PC T-girder bridge", *Proceedings of the 6th Symposium on the Use of Composite Structure*, pp. 1-8. [In Japanese]

Gardner, N.J. and Lockman, M.J. (2001), "Design provisions for drying shrinkage and creep of normal-strength concrete", *ACI Mater. J.*, **98**(2), 159-167.

Geng, Y., Wang, Y.Y., Ranzi, G. and Wu, X.R. (2014), "Time-dependent analysis of long-span, concrete-filled steel tubular arch bridges", *J. Bridge Eng.*, *ASCE*, **19**(4), 04013019-1-9.

Ikeda, H., Kutsuna, Y., Sekii, K. and Ito, Y. (2002), "Design of PC corrugated steel web box girder bridges of Nabeta-west project in new Meishin express way", *Proceedings of the 1st Fib Congress*, *Session 5*: *Composite Structures*, Osaka, Japan, Japan Concrete Institute (JCI), pp. 323-328.

Jiang, R.J., Au, F.T.K. and Xiao, Y.F. (2015), "Prestressed Concrete Girder Bridges with Corrugated Steel Webs: Review", *J. Bridge Eng.*, *ASCE*, **141**(2), 04014108-1-9.

Johnson, R.P. and Cafolla, J. (1997), "Corrugated webs in plate girders for bridges", *Proceedings of the Institution of Civil Engineers*: *Structures and Buildings*, **122**(2), 157-164.

Jung, K.H., Kim, K.S., Sim, C.W. and Kim, J.H.J. (2011), "Verification of incremental launching construction safety for the Ilsun Bridge, the world's longest and widest prestressed concrete box girder with corrugated steel web section", *J. Bridge Eng.*, *ASCE*, 453-460.

Kano, M., Yamano, T., Nibu, M. and Kitada, T. (1997), "A computer program, USSP, for analyzing ultimate strength of steel plated structures", *Proceedings of 5th International Colloquium on Stability and Ductility of Steel Structures*, Japanese Society of Steel Construction, Tokyo, Japan, pp. 763-770.

Liu, X.G., Fan, J.S., Bai, Y., Tao, M.X. and Nie, J.G. (2015), "Stress increment of unbonded prestressing tendons in prestressed concrete girders with corrugated steel webs", *J. Bridge Eng.*, *ASCE*, **20**(7), 04014094-1-11.

Lou, T.J., Lopes, S.M.R. and Lopes, A.V. (2015), "Interaction between time-dependent and second-order effects of externally posttensioned members", *J. Bridge Eng.*, *ASCE*, **20**(11), 06015003-1-8.

Machimdamrong, C., Watanabe, E. and Utsunomiya, T. (2004), "Analysis of corrugated steel web girders by an efficient beam bending theory", *Struct. Eng. Earthq. Eng.*, **21**(2), 131-142.

Mizuguchi, K., Ashiduka, K., Yoda, T., Sato, K., Sakurada, M. and Hidaka, S. (1998), "Loading tests of Hondani Bridge", *Bridge Found. Eng.*, **32**(10), 25-34. [In Japanese]

Mo, Y.L. and Fan, Y.L. (2006), "Torsional design of hybrid concrete box girders", *J. Bridge Eng.*, *ASCE*, **11**(3), 329-339.

Neville, A.M. (1996), *Properties of concrete*, (4th Edition), John Wiley & Sons, New York, NY, USA.

Podolny, W. (1985), "The cause of cracking in post-tensioned concrete box girder bridges and retrofit procedures", *PCI Journal*, **30**(2), 82-139.

Roesler, H. and Denzer, G. (2002), "The prestressed concrete bridge Altwipfergrund with corrugated steel webs", *Proceedings of the 1st fib Congress*, *Session 5*: *Composite structures*, Osaka, Japan, pp. 339-346.

Rosignoli, M. (1999), "Prestressed concrete box girder bridges with folded steel plate webs", *Proceedings of the Institution of Civil Engineers-Structures and Buildings*, **134**(1), 77-85.

Shiratani, H., Sakashita, K., Obi, H. and Fujikura, S. (2002), "Behavior of corrugated steel web girder around middle support", *Proceedings of the 1st fib Congress*, *Session 5*: *Composite structures*, Osaka, Japan, pp. 261-268.

Sprinkel, M.M. and Balakumaran, S.S. (2017), "Problems with continuous spliced posttensioned-prestressed concrete bulb-tee girder center spans at west point, Virginia", *Transport. Res. Record*, **2642**, 46-54.

Sung, Y.C., Lin, T.K., Chiu, Y.T., Chang, K.C., Chen, K.L. and Chang, C.C. (2016), "A bridge safety monitoring system for prestressed composite box-girder bridges with corrugated steel webs based on in-situ loading experiments and a long-term monitoring database", *Eng. Struct.*, **126**, 571-585.

Wan, S., Li, S.Q. and Ma, L. (2009), "Application of prestressed concrete composite box-girder structure with corrugated steel webs in bridge engineering in China", *J. Archit. Civ. Eng.*, **26**(2), 15-20. [In Chinese]

Xiao, Y., Li, L. and Yang, R.Z. (2014), "Long-term loading behavior of a full-scale Glubam bridge model", *J. Bridge Eng.*, *ASCE*, **19**(9), 04014027-1-7.

Yamaguchi, K., Yamaguchi, T. and Ikeda, S. (1997), "The mechanical behavior of composite prestressed concrete girders with corrugated steel webs", *Concr. Res. Technol. JCI*, **8**(1), 27-40. [In Japanese]

Zhan, Y.L., Zhao, R.D., Ma, Z.G., Xu, T.F. and Song, R.N. (2016a), "Behavior of prestressed concrete-filled steel tube(CFST) beam", *Eng. Struct.*, **122**, 144-155.

Zhan, Y.L., Ma, Z.G., Zhao, R.D., Li, G.F. and Xiang, T.Y. (2016b), "Interface Behavior between Steel and Concrete Connected by Bonding", *ASCE*, *J. Bridge Eng.*, **21**(6), 04016026.

CC